Macromolecules

pubs.acs.org/Macromolecules Article

Ionomers from Step-Growth Polymerization: Highly Ordered Ionic Aggregates and Ion Conduction

Lu Yan, Lauren Hoang, and Karen I. Winey*

Cite This: *Macromolecules* 2020, 53, 1777−1784 Read Online

ACCESS | Metrics & More | Article Recommendations | Supporting Information

ABSTRACT: Precisely controlling the position of ionic groups along neutral polymer backbones in ionomers has led to novel nanoscale morphologies and promising properties, although the synthetic routes can be quite demanding. Here, we report a series of Li^+-containing ionomers directly synthesized from step-growth polymerization of commercially available diol monomers (x = 6 or 12) and dianhydride monomers followed by neutralization with various amounts of lithium salts. The results are nearly precise linear polymers wherein nonpolar segments have precisely 6 or 12 methylene groups, as determined by the diol. The functional segment has two carboxylic acid pendant groups and 6−8 backbone atoms depending on the dianhydride addition. From X-ray scattering, these segmented ionomers exhibit well-defined nanostructures in contrast to the conventional random ionomers. The nearly precise nature of these segmented ionomers does not compromise the morphological ordering. The temperature-dependent ionic conductivities exhibit a systematic increase with Li^+ neutralization level, as expected in a single-ion conductor. Notably, the ionic conductivities in these amorphous ionomers at high neutralization levels (≥65%) exhibit Arrhenius behavior even at $T > T_g$, suggesting that ion mobility is decoupled from polymer segmental motion and largely within the aggregates; this finding could be a promising design strategy for solid polymer electrolytes. The synthetic scheme reported here provides a readily accessible suite of nearly precise ionomers by which to build fundamental correlations between polymer microstructures, nanoscale ionic aggregate morphologies, and ionic conductivities that are currently lacking.

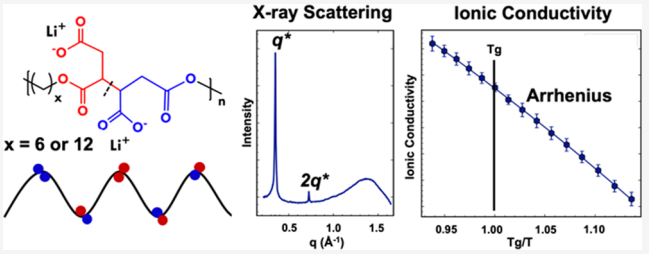

INTRODUCTION

Rechargeable lithium-ion batteries are one of the most widely used battery systems and are an important component in the growing clean energy landscape.[1−4] The development of solid polymer electrolytes (SPEs) to replace liquid electrolytes is essential as they are inherently safer and have the potential to be multifunctional.[5−8] Compared to a conventional polymer lithium salt system, single-ion conductors, where anions are covalently bonded to the polymer backbones, can overcome the low transference number and concentration polarization issues that arise from free anion migration.[9−12] Ionomers are one type of single-ion conductors that contain a small fraction of covalently bonded ionic groups.[13,14] The nanoscale phase separation in ionomers, which is due to the high dielectric constant of the ionic groups compared to the low dielectric constant polymer backbone, gives rise to various shapes and connectivities (spherical, stringy, and percolated) of the ionic aggregates.[15−17]

Extensive studies have demonstrated that the ion transport in ionomers is coupled with polymer segmental motion at temperatures higher than the glass transition temperature (T_g).[18−25] Conductivity requires the availability of charge carriers and the high mobility of these carriers, thus requiring high chain mobility. Consequently, one well-established method to enhance ion conduction is to lower the glass transition temperature,[12,26−28] although, decreasing the T_g to promote ion transport leads to a reduction in the mechanical properties of SPEs.[5,29−31] Circumventing this trade-off requires the optimization of both mechanical strength and ionic conductivity. Additional fundamental knowledge of how ionic aggregate morphology affects ion transport in ionomers could resolve the long-standing limitation in SPEs.

We have been working to elucidate the connection between aggregate morphologies and properties using a series of precise polyethylene (PE)-based precise acid or ion-containing polymers synthesized via acyclic diene metathesis (ADMET).[32−36] ADMET is a polycondensation reaction. Starting from terminal olefin monomers and the metallic methylidene catalyst, metal alkylidene and ethylene condensates are formed through metathesis reaction. The newly formed metal alkylidenes react further with a second terminal olefin molecule producing growing polymers. The ADMET reaction is fully reversible at each step, and therefore constantly removing ethylene condensates pushes the reaction equili-

Received: October 21, 2019
Revised: January 24, 2020
Published: February 17, 2020

https://dx.doi.org/10.1021/acs.macromol.9b02220
Macromolecules 2020, 53, 1777−1784

brium toward the chain growth.[37−41] In contrast to randomly functionalized copolymers, these precise polymers exhibit remarkably uniform nanoscale morphologies that enable us to understand the morphological effect on mechanical properties or ion transport.[34,35,42−49] In conjunction with experimental studies, both coarse-grained (CG) and all-atom (AA) molecular dynamics (MD) simulations have been used to investigate the morphologies and dynamics of these precise ionomers.[36,42,43,50−52] The CG and AA MD simulation results in these precise PE-based ionomers show excellent agreement with X-ray scattering data and further reveal various ion aggregate morphologies including compact-isolated, branched-stringy, and percolated morphologies as the PE-segment length decreases or the neutralization level increases.[36,50,51] Further MD studies show that percolated ionic aggregate morphologies exhibit higher conductivities in comparison with the discrete aggregates[53,54] and the ion diffusivity within the aggregates exhibits superionic transport that is decoupled from polymer segmental dynamics as evidenced by various CG and AA MD simulations.[52,55] Therefore, producing percolated ionic aggregates within single-ion conducting polymers is a promising route to decouple the ion transport from the polymer segmental dynamics and to increase ionic conductivity without compromising mechanical properties.[56] Although the PE-based precise ionomers produce well-defined nanoscale morphologies and even percolated aggregates for efficient ion pathways, the ADMET synthesis currently imposes severe constraints on polymer quantities that impedes further experimental investigations.

A recent study on morphology characterization of a series of nearly precise ionomers, where the acid groups are separated by either n or $n + 1$ methylene group, also observed well-defined morphologies and showed that the nearly precise ionomers are essentially indistinguishable from the strictly precise polymers.[57] That preliminary study investigated just one polymer system with a single ion content. Building upon that promising study, we report herein a scalable synthesis for a new series of nearly precise acid-containing polymers and their neutralization with lithium salts. These newly designed ionomers contain twice as many acid groups in the repeating unit comparing to the previously studied precise ionomers, so that this polymer provides more neutralization sites to achieve higher Li^+ contents. The degree of acid group neutralization varies from ∼15 to 80%, allowing a systematic study of the ion content effects on aggregate morphology and ion transport. These nearly precise ionomers at high levels of neutralization exhibit highly ordered ionic aggregate morphologies and decoupled ion conductivities from polymer segmental dynamics at $T > T_g$.

EXPERIMENTAL SECTION

Materials. From Sigma-Aldrich, 1,6-hexanediol and 1,12-dodecanediol, lithium acetate, and lithium *tert*-butoxide [2 M in tetrahydrofuran (THF)] were purchased. Prior to storage in a glovebox, 1,6-hexanediol and 1,12-dodecanediol and lithium acetate were dried under vacuum at 60 °C overnight to remove water. From TCI and Alfa Aesar, respectively, 1,2,3,4-butanetetracarboxylic dianhydride (>96%) and pyridine (anhydrous, >99.5%, sealed in argon) were purchased. Water-sensitive chemicals are stored in the argon-filled glovebox.

Synthesis of Carboxylic Acid-Containing Polymers. The nearly precise carboxylic acid-containing polymers were synthesized by step-growth polymerization of 1,6-hexanediol or 1,12-dodecanediol and 1,2,3,4-butanetetracarboxylic dianhydride. A 1:1 molar ratio of monomers was added into the flask in the glovebox followed by adding 20 wt % anhydrous pyridine as a solvent. The reaction was stirred at 85 °C for 6 h under an argon environment until the magnetic stirring stopped due to the high viscosity of the products. The resulting polymers were then dissolved in THF and were precipitated into cold hexane to remove unreacted diol monomers. The precipitated polymers were filtrated followed by vacuum drying at 40 °C overnight to remove the residual solvent. The polymers are named PExBA, where x = 6 or 12 indicates the number of carbons in the starting diol molecules.

Synthesis of Lithium Carboxylate Ionomers. The nearly precise lithium carboxylate ionomers were prepared by neutralizing the corresponding acid-containing polymers. The neutralization procedure started by dissolving PE6BA or PE12BA polymers in THF at a concentration of ∼5 wt %. A stoichiometric amount of dried lithium acetate or lithium *tert*-butoxide THF solution (∼5 wt %) was then added dropwise into the polymer THF solution. The reaction was stirred for 2 h at room temperature. The resulting neutralized polymers are precipitated from solution, and the products were recovered via vacuum filtration. Dialysis was then performed in deionized (DI) water to remove the excess amount of lithium salts by using the dialysis tube with 2 kDa cutoff molecular weight (Millipore Sigma). The extent of neutralization achieved from this neutralization process was determined by the elemental analysis at Galbraith Laboratories (Knoxville, TN) on C, H, and Li from ∼50 mg of samples. The error in the reported neutralization mole percentage is ∼±5% (Table S1). Note that the level of neutralization was higher when using lithium *tert*-butoxide due to its higher pkA. The neutralized samples are denoted with nLi, where n is the percentage of carboxylic acid groups that are neutralized.

Material Characterization. All ^{1}H NMR (360 MHz) spectra were recorded in DMSO-d_6 [D, 99.9%, with ±0.05 v/v tetramethylsilane (TMS), Cambridge Isotope Laboratories, Inc.] on a Bruker DMX 360 NMR spectrometer with 32 scans at 25 °C. The data is analyzed using the Topspin 3.5 pl 7 software. NMR spectra are provided in Figures S1 and S2.

Fourier transform infrared (FTIR) was performed on a Thermo Scientific Nicolet iS5 spectrometer at room temperature with 2 cm^{-1} resolution and 32 scans. Polymer water solutions were drop cast onto silicon wafers and dried prior to FTIR scans. After subtracting the silica background, curves were normalized by the C−H bending absorption peak at 1466 cm^{-1} after subtracting the silica background.

Polymer molecular weights and dispersity (Figure S3) were determined by using a Tosoh EcoSEC GPC with a dual-flow refractive index detector. The gel permeation chromatography (GPC) was configured with three single-pore gel columns (Tosoh) at 40 °C, with high-performance liquid chromatography (HPLC) grade THF (Sigma-Aldrich) as the mobile phase at a flow rate of 1 mL/min. The injection was made at ∼0.05 wt % sample concentration with 500 μL injection volume. The retention time was calibrated using narrow-molecular-weight polystyrene standards (Sigma-Aldrich, Polystyrene low molecular Standard ReadyCal Set: M_p from 250 to 70 000 g/mol). Standards were selected to include M_p covering the expected polymer range.

Differential scanning calorimetry (DSC) measurements were performed on a TA Instruments Q2000 digital scanning calorimeter. The 5−10 mg polymer samples were dried in a vacuum oven at 60 °C overnight and sealed in hermetic pans prior to DSC measurement. Dried samples were equilibrated at 25 °C in DSC, then heated to 150 °C to remove thermal history, and then cooled to −20 °C followed by heating back to 150 °C with 10 °C/min ramp rate. The glass transition temperature was determined by the inflection point of the change in heat flow from the second heating scan via Universal Analysis. DSC thermograms are provided in Figure S5.

X-ray scattering data were acquired in the multiangle X-ray scattering (MAXS) facility at the University of Pennsylvania with a Cu Kα source with a wavelength of 1.54 Å. The scattering data were collected for 30 min at a sample-to-detector distance of 11 cm. Samples prepared for X-ray scattering were melt-pressed in a Carver 4122 hot press at 100 °C for 10 min and were stored in an evacuated

https://dx.doi.org/10.1021/acs.macromol.9b02220
Macromolecules 2020, 53, 1777−1784

desiccator at room temperature prior to experiments. Two-dimensional data reduction and analysis of data were performed using the Datasqueeze software.

Ionic conductivity measurements were carried out via electrochemical impedance spectroscopy (EIS). Samples were prepared by drop casting the ionomer water solution onto 20 mm diameter stainless steel electrodes with two 100 μm silica spacers. Water was evaporated to form a thin film on the electrode, and the polymer films were then placed in a vacuum oven at room temperature overnight to remove moisture. The dried sample films were sandwiched between two parallel electrodes with a 10 mm diameter electrode on top. Impedance spectra were measured using a Solartron Analytical Modulab XM MTS spectrometer in a Janis VPF-100 cryostat, with a frequency range of 10^{-1}–10^{6} Hz at an amplitude of 100 mV. Samples were annealed at 97 or 127 °C until equilibrium was reached in the cryostat and were measured every 5 °C upon cooling after a 10 min hold at each measured temperature. The bulk resistance of the sample (R) was determined by fitting the Nyquist plot with an equivalent circuit composed of constant phase elements (CPE) and a resistor via the XM-studio software. Details of impedance data fitting are provided in the Supporting Information. The ionic conductivity was then calculated using equation

$$\sigma = \frac{l}{R \times A}$$

where l is the sample thickness and A is the electrolyte area.

RESULTS AND DISCUSSION

Polymer Synthesis. Figure 1 shows the step-growth polymerization of 1,6-hexanediol or 1,12-dodecanediol and

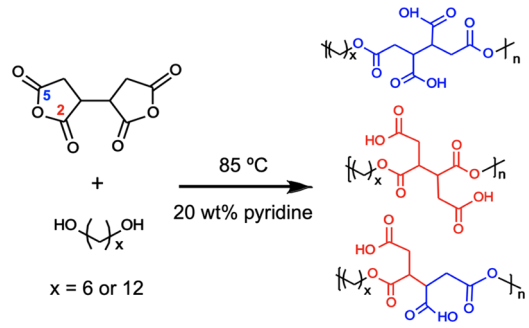

Figure 1. Reaction scheme of PExBA polymers (x = 6 or 12). The blue and red colors represent nucleophilic attacks at the C2 and C5 carbonyl carbons, respectively, of the 1,2,3,4-butanetetracarboxylic dianhydride.

1,2,3,4-butanetetracarboxylic dianhydride to produce the nearly precise carboxylic acid-containing polymer. The hydroxyl groups in the diol molecules attack either the second or fifth carbonyl carbons in the 1,2,3,4-butanetetracarboxylic dianhydride molecules, therefore, the resulting polymer has a mixed chemical structure of proximal and distal carboxylic acid units.[58] Anhydrous pyridine was added at 20 wt % as a catalyst to avoid further reactions of diol and the pendant carboxylic acid groups. When the reactions were conducted at temperatures higher than 120 °C for over 6 h, insoluble polymers resulted, indicating cross-linking. Therefore, the reaction conditions used were 85 °C for 6 h to prevent cross-linking. The ^{1}H NMR spectra provided in Figure S1 show no evidence of cross-linking from the hydrogen integration numbers in ^{1}H NMR spectra and polymers dissolve in THF or DMSO at room temperature. The number-averaged molecular weights (M_n) and the dispersity ($Đ$) were determined by GPC and are listed in Table 1. The volume fraction of pendant carboxylic

Table 1. Physical Properties of PExBA Polymers

polymers	DP_n	Φ_{acid}[a]	M_n [kg/mol]	dispersity ($Đ$)	T_g [°C]
PE6BA	32.9	0.27	10.8	2.4	8.7
PE12BA	28.5	0.20	11.4	2.2	−3.3

[a]Volume fractions of acid groups are calculated from van der Waals volume via the Chemicalize software.

acid groups is 0.27 for PE6BA and 0.20 for PE12BA. Here, PE12BA has a comparable acid group volume fraction to p9AA (Φ_{acid} = 0.20), where carboxylic acid groups are placed on every ninth carbon along the PE backbone.[35] These nearly precise acid-containing polymers were neutralized with lithium cations, and the extent of Li^+ neutralization on the acid groups ranges from 14 to 80% as determined from the elemental analysis. The wide range of lithium-ion neutralization levels allows a systematic study of the relationship between ion content and morphologies, as well as ion-transport properties.

FTIR and Thermal Properties. To confirm the neutralization, FTIR spectra of the nearly precise polymers before and after Li^+ neutralization are compared in Figure 2. Full spectra

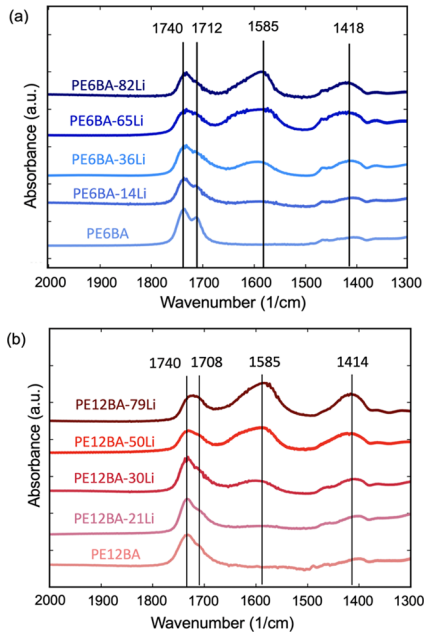

Figure 2. Comparison of FTIR between (a) PE6BA and (b) PE12BA polymers before and after Li^+ neutralization.

are provided in Figure S4. The absorption bands at ∼1740 and ∼1710 cm^{-1} in PE6BA and PE12BA correspond to the C═O stretching vibration from the ester groups and the dimer form of carboxylic acid groups in PE6BA and PE12BA. After neutralizing the carboxylic acid groups with Li^+, new absorption bands at 1585 and ∼1415 cm^{-1} appear, which arise from the asymmetric stretching mode of negatively charged carboxylate groups.[59] The relative intensity of the absorption bands at 1585 and ∼1415 cm^{-1} increases with the degree of neutralization, thereby reflecting more negatively charged carboxylate groups appear in the polymers. The decrease in the absorption band intensity at ∼1710 cm^{-1}, indicating the decreased dimer-form −COOH contents, further confirms the increased neutralization level in the polymers.

https://dx.doi.org/10.1021/acs.macromol.9b02220
Macromolecules 2020, 53, 1777−1784

DSC was performed on all materials to investigate the effect of the ion content on thermal properties. All polymers are amorphous and only exhibit a single glass transition temperature regardless of the ion content, see Figure S5. The short methylene sequences (6 or 12 carbons), the presence of associating acid or ionic groups, and tacticity impede the crystallization of these nearly precise polymers. Figure 3

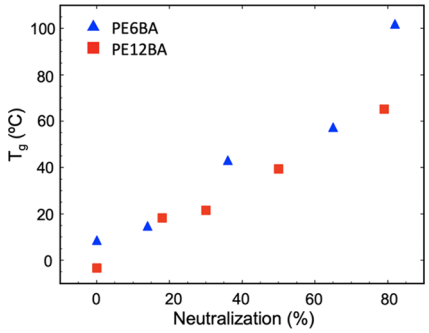

Figure 3. Glass transition temperature (T_g) versus the Li^+ neutralization level in PE6BA and PE12BA polymers.

displays the correlation between T_g and neutralization levels in PE6BA and PE12BA ionomers. The methylene sequence length (6 or 12) has a modest influence on T_g relative to the strong dependence on the ion content in these polymers. The shorter methylene spacer lengths exhibit a slightly higher glass transition temperature at 0% Li: −3.3 °C for PE6BA and 8.7 °C for PE12BA. The glass transition temperatures of the ionomers increase dramatically and monotonically with the neutralization level, particularly for PE6BA-82Li (T_g = 102 °C). The high level of acid and ionic aggregation in the highly neutralized ionomers gives rise to the reduced chain mobility, which is reflected in an increase in T_g.

Room-Temperature Morphologies. X-ray scattering reveals the effect of lithium neutralization on the morphologies of PE6BA and PE12BA ionomers, Figure 4. The peak positions

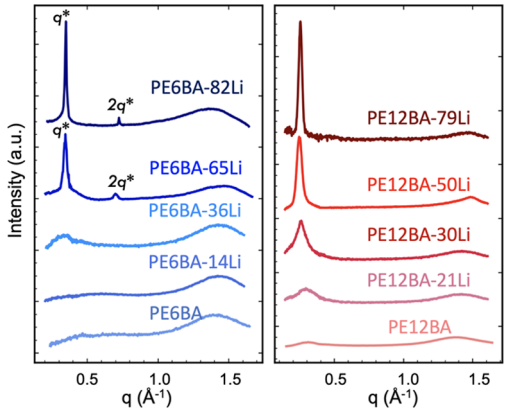

Figure 4. Room-temperature X-ray scattering data of PE6BA (left) and PE12BA (right) polymers. Data are shifted vertically for clarity.

were extracted by fitting with pseudo-Voigt functions (Figures S6 and S7), and the fitting parameters are provided (Table S2). All materials exhibit an isotropic and broad peak at $q \sim 1.4$ Å^{-1} that arises from amorphous polymer backbone scattering, thereby confirming the lack of crystallinity in PE6BA and PE12BA polymers observed by DSC. The ionomer peaks in the lower q-range (q^* = 0.1−0.7 Å^{-1}) correspond to the average distances between acid or ionic aggregates ($d_{aggregates}$). For nominally spherical aggregates, $d_{aggregate}$ corresponds to the average center-to-center interaggregate distance, while for fully percolated aggregates, $d_{aggregate}$ corresponds to the average branch-to-branch intra-aggregate distance.

Prior to neutralization, the broad scattering features in PE6BA (q^* = 0.69 Å^{-1}) and PE12BA (q^* = 0.30 Å^{-1}) correspond to the average distances between aggregates comprised of hydrogen-bonded carboxylic acid groups assembled with liquid-like order. Previous studies show that acid-containing polyethylenes with pseudorandom placement of the acid groups do not exhibit acid aggregate peaks due to the lack of nanoscale structural uniformity that arises when the pendant groups along the polymer backbone are irregularly spaced.[32] In contrast, PE6BA and PE12BA with the well-defined placements of the pendant groups give rise to better-defined aggregate morphologies leading to the low-q peaks in X-ray scattering. Upon neutralization, the low-q peaks become more intense compared to the acid form of the polymers as a result of the higher electron density contrast. Interestingly, a second-order peak with a 1:2 q-ratio appears in the highly neutralized PE6BA ionomers (PE6BA-65Li and PE6BA-82Li), suggesting exceptional uniformity in the ionic aggregate morphologies even in the absence of crystallinity. The origin of this second-order peak requires further investigation, particularly using all-atom molecular dynamics simulations, to ascertain the aggregate shape and packing.

Figure 5a shows the average $d_{aggregate}$ as a function of neutralization. At a fixed level of neutralization, increasing the

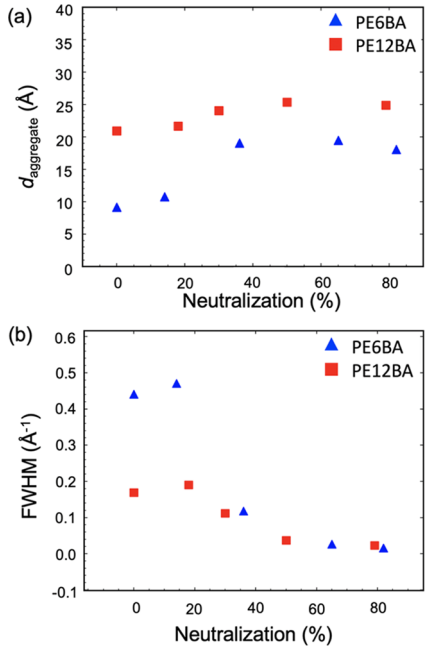

Figure 5. Analysis of the low-angle X-ray scattering peak as a function of neutralization level in PE6BA and PE12BA: (a) average distances and (b) full width at half maximum (FWHM) of the low-angle peaks.

alkyl spacer length from 6 to 12 leads to larger $d_{aggregate}$, as expected. This trend is more profound for polymers at low neutralization levels (0−25%), e.g., $d_{aggregate}$ in PE12BA and PE12BA-21Li (~22 Å) is about twice the distances in PE6BA and PE6BA-14Li (~10 Å). The longer alkyl spacer increases

https://dx.doi.org/10.1021/acs.macromol.9b02220
Macromolecules 2020, 53, 1777−1784

the spacing between ionic or acid groups along the polymer backbone, which increases the $d_{aggregate}$. Note that the impact of the spacer length is smaller at higher levels of neutralization, although this is difficult to interpret without knowing the aggregate shapes and symmetries.

At a fixed spacer length, increasing the degree of neutralization up to ~45% increases $d_{aggregate}$, while at higher levels of neutralization, $d_{aggregate}$ is nominally independent of the degree of neutralization. The increase in the interaggregate distance between the acid form and modest levels of neutralization is likely the result of an increase in the aggregate sizes. All-atom MD simulations of similar polymers (precise poly(ethylene-*co*-acrylic acid) ionomers with Φ_{acid} = 0.13−0.20) have shown that in the acid form (0% neutralization), the acid groups form small aggregates with only a few acid groups (2 or 3 typically), while neutralization with Li^+ drives the formation of larger aggregates associated with stronger electrostatic interactions.[51,60,61] After this initial increase in the aggregate size and the corresponding increase in $d_{aggregate}$ with neutralization, the $d_{aggregate}$ and the aggregate size appear to become independent of neutralization, although the peak intensity increases continuously with neutralization. The recent all-atom MD simulations reveal that increasing the neutralization level has little impact on the $d_{aggregate}$, as we observe here.[36,51] Rather, the simulations find that the connectivity of the ionic aggregates increases, i.e., stringy aggregates become branched and eventually percolate. Because PE12BA and PE6BA contain comparable Φ_{acid} (0.20−0.27), we expect a similar increase in the ionic aggregate connectivity at >45% neutralization where $d_{aggregate}$ is nominally independent of the neutralization level.

The transitions in $d_{aggregate}$ are commensurate with changes in the ionomer peak widths with the neutralization level, Figure 5b. When the neutralization level of PE6BA increases from 0 to ~45%, the full width at half maximum (FWHM) of the low-q peaks dramatically drops from ~0.45 to ~0.02 $Å^{-1}$. PE12BA exhibits a less pronounced decrease. The unusually sharp peaks in highly neutralized PE6BA and PE12BA ionomers arise from the uniform periodicity of the pendant groups on the backbone and the high ion contents, which both contribute to the high packing order of the aggregates.[57] For context, when the ion content is low due to partial neutralization, the ionic aggregates in amorphous polymers with pendant functional groups are nominally spherical and the X-ray scattering pattern exhibits just one peak with a larger full width half maximum (FWHM) of ~0.10 $Å^{-1}$.[51] The narrow peak widths shown in Figure 5b are comparable to that reported for a semicrystalline polymer with periodic ionic layers.[47] Until the shape of the ionic aggregates can be determined using all-atom molecular dynamics simulations or a direct imaging method, our discussion of the morphology and property correlations will remain speculative.

Ionic Conductivities. The ion transport properties of PE6BA and PE12BA ionomers were examined as a function of temperature, Figure 6. The ionic conductivities (σ_{DC}) increase by about one order of magnitude from PE12BA to PE6BA ionomers at similar degrees of neutralization, which is consistent with the higher total number of ions at a given neutralization level in the PE6BA ionomers. At a fixed temperature (Figure 6a), increasing the neutralization level above 25% in either PE6BA or PE12BA leads to an order of magnitude increase in ionic conductivities. This change in the ionic conductivities occurs concurrently with the changes in

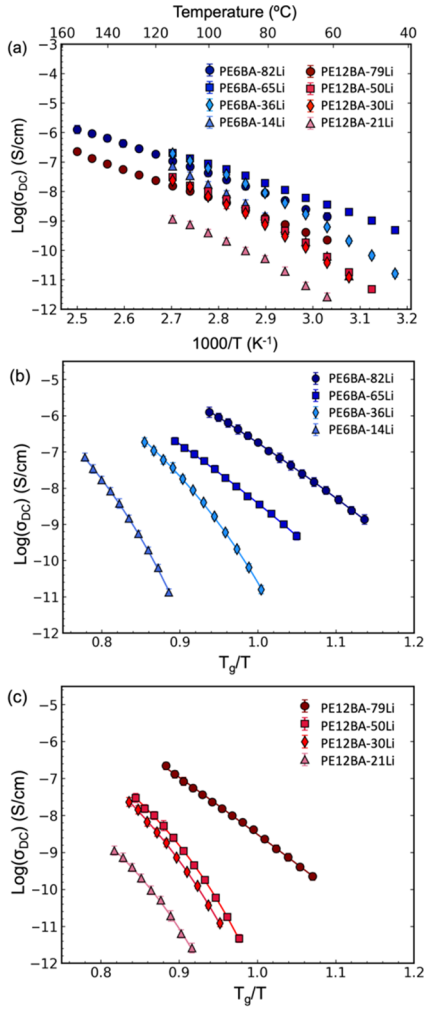

Figure 6. Ionic conductivity of Li-neutralized PE6BA and PE12BA ionomers as a function of (a) $1/T$ and (b, c) T_g/T. Solid lines are fits to VFT behavior at lower neutralization levels (≤50%) and to Arrhenius behavior at higher neutralization levels (≥65%).

$d_{aggregate}$ and FWHM (Figure 5). Thus, we attribute this increase in σ_{DC} mainly to a change in ionic aggregate size and composition. Further increasing the neutralization level, where we suspect an increase in ionic aggregate connectivity, does not significantly increase the conductivity at a fixed temperature as measured by electrochemical impedance spectroscopy.

The T_g normalized σ_{DC} of PE6BA and PE12BA ionomers are shown in Figure 6b,c. The ionic conductivities systematically increase with the neutralization level in both PE6BA and PE12BA ionomers. This trend could result from both higher total ion content and changes in the ionic aggregate morphologies with increasing neutralization levels. The ionic conductivities of ionomers with ≤50% Li-neutralization are well described with the Vogel−Tammann−Fulcher (VTF) equation

$$\sigma = \sigma_0 \exp\left(\frac{-D}{R(T-T_0)}\right)$$

where σ_0 is the ionic conductivity at an infinitely high temperature, T_0 is the Vogel temperature, and D is reciprocally related to fragility. Fitting parameters are summarized in Table S3. This VFT temperature-dependence behavior suggests that

https://dx.doi.org/10.1021/acs.macromol.9b02220
Macromolecules 2020, 53, 1777−1784

ion transport in ionomers with ≤50% Li-neutralization is coupled with polymer chain segmental dynamics at $T > T_g$. Notably, σ_{DC} in ionomers with ≥65% Li-neutralization (PE6BA-82Li, PE6BA-65Li, and PE12BA-79Li) exhibits Arrhenius-like behavior even at $T > T_g$, which implies a decoupling of the ion transport from the polymer backbone dynamics. Recent all-atom MD simulations of fully neutralized precise poly(ethylene-*co*-acrylic acid) ionomers with percolated ionic aggregates[50,51] found that Li^+ motion inside aggregates is faster than the polymer segmental relaxation.[51,55] Given that the nearly precise ionomers studied here are chemically similar, we infer that the decoupling of ion transport from the chain segmental motion found in PE6BA-82Li, PE6BA-65Li, and PE12BA-79Li arises from high connectivity of the ionic aggregates.

To extend our analysis to the effect of the ion content, we extract the reduced conductivity at 20 K above T_g for each ionomer as a function of neutralization (Figure 7). The T_g + 20 K was chosen because all materials were tested at such temperature. We observe that the reduced ionic conductivities at T_g + 20 K increase with the neutralization level monotonically, demonstrating that higher ion concentrations give rise to higher ionic conductivity. The fact that PE6BA ionomers have almost an order of magnitude higher conductivity compared to PE12BA ionomers at similar neutralization level correlates to their higher ion concentrations. The ionic conductivities in PE6BA and PE12BA ionomers correlate strongly with the ion content, which suggests that the morphological changes in the ionic aggregates are gradual in these amorphous materials. At T_g + 20 K, the highest ionic conductivity is found in the ionomer with the shorter alkyl spacer and the highest neutralization level. Nonetheless, the ionic conductivities in these materials are still limited due to the strong electrostatic interaction between carboxylate anions and the lithium cations. Future efforts to enhance the ionic conductivities in ionomers will involve facilitating counterion dissociation within percolated ionic aggregates.

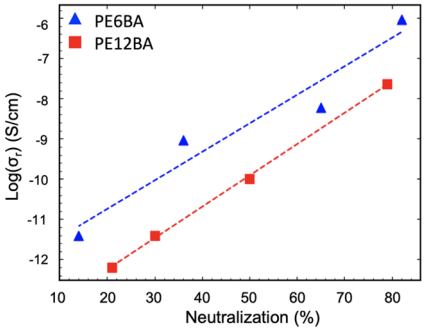

Figure 7. Reduced ionic conductivity (σ_r) of PE6BA and PE12BA ionomers as a function of neutralization level at T_g + 20 K. The dashed lines are linear fits.

CONCLUSIONS

We have synthesized a series of new acid-containing polymers using step-growth polymerization of commercially available diol (x = 6 or 12) and dianhydride monomers and have subsequently neutralized these nearly precise polymers with lithium ions. This synthetic route provides easy access to scalable reactions. As evidenced by X-ray scattering, these new ionomers exhibit well-defined amorphous nanostructures that are reminiscent of morphologies previously found in precise amorphous ionomers made by ADMET. Interestingly, the PE6BA ionomers at high levels of neutralizations (PE6BA-65Li and PE6BA-82Li) exhibit a second-order ionomer peak indicating exceptional nanoscale uniformity of the ionic aggregates, which is absent in conventional ionomers with random ionic group functionalization.

The ionic conductivities of these nearly precise ionomers increase with the neutralization content. The ionomers with a low ion content (≤50%) exhibit Vogel−Fulcher−Tammann (VFT) behavior in ion conduction, suggesting that the ion transport is facilitated by polymer chain segmental motion at $T > T_g$ and probably involves the merger and separation of distinct ionic aggregates. In contrast, highly neutralized ionomers (≥65%) exhibit Arrhenius-like conductivity even at $T > T_g$, indicating that ion transport is decoupled from the polymer segmental motion and suggesting that ion motion predominately occurs within highly extended, perhaps even percolated, ionic aggregates.

Given the accessibility of the polymerization route, future investigations of segmented ionomers to explore the impact of the methylene spacer length and the cation type will be straightforward. Changing the spacer length might lead to new ordered ionic aggregate morphologies, such as layered, cubical, or hexagonal symmetry, as recently reported in other segmented ionomers from polycondensation reactions.[62,63] To date, the effect of ionic aggregate morphologies on ion transport is poorly understood in single-ion conductors due largely to the lack of available synthetic schemes that produce well-defined polymer molecular structures and well-defined ionic aggregate morphologies. This study opens the possibilities to systematically explore fundamental questions of the relationship between ionic aggregate morphologies and ion conduction and thereby improve ion conductivity in single-ion conducting polymer electrolytes.

ASSOCIATED CONTENT

Supporting Information

The Supporting Information is available free of charge at https://pubs.acs.org/doi/10.1021/acs.macromol.9b02220.

^{1}H NMR spectra; GPC chromatograms; elemental analysis results; FTIR spectra; DSC thermograms; fitting of X-ray scattering profiles; fitting example of a representative EIS data; fitting parameters for ionic conductivity data (PDF)

AUTHOR INFORMATION

Corresponding Author

Karen I. Winey − *Department of Chemical and Biomolecular Engineering and Department of Materials Science and Engineering, University of Pennsylvania, Philadelphia, Pennsylvania 19104-6315, United States;* orcid.org/0000-0001-5856-3410; Email: winey@seas.upenn.edu

Authors

Lu Yan − *Department of Chemical and Biomolecular Engineering, University of Pennsylvania, Philadelphia, Pennsylvania 19104-6315, United States;* orcid.org/0000-0002-5248-7821

https://dx.doi.org/10.1021/acs.macromol.9b02220
Macromolecules 2020, 53, 1777−1784

Lauren Hoang − *Department of Materials Science and Engineering, University of Pennsylvania, Philadelphia, Pennsylvania 19104-6315, United States*

Complete contact information is available at: https://pubs.acs.org/10.1021/acs.macromol.9b02220

Notes

The authors declare no competing financial interest.

■ ACKNOWLEDGMENTS

We acknowledge the funding from NSF-DMR 1506726 and 1904767. We thank Dr. Dale Huber and Dr. Amalie Frischknecht at Sandia National Laboratories, for many productive discussions on the chemistry and structures. We also thank Dr. Edward B. Trigg and Ben Paren on the discussion about ionomers.

■ REFERENCES

(1) Li, M.; Lu, J.; Chen, Z.; Amine, K. 30 Years of Lithium-Ion Batteries. *Adv. Mater.* **2018**, *30*, No. 1800561.
(2) Tarascon, J.-M.; Armand, M. Issues and Challenges Facing Rechargeable Lithium Batteries. *Nature* **2001**, *414*, 359−367.
(3) Whittingham, M. S. Lithium Batteries and Cathode Materials. *Chem. Rev.* **2004**, *104*, 4271−4301.
(4) Winter, M.; Barnett, B.; Xu, K. Before Li Ion Batteries. *Chem. Rev.* **2018**, *118*, 11433−11456.
(5) Hallinan, D. T.; Balsara, N. P. Polymer Electrolytes. *Annu. Rev. Mater. Res.* **2013**, *43*, 503−525.
(6) Sun, C.; Liu, J.; Gong, Y.; Wilkinson, D. P.; Zhang, J. Recent Advances in All-Solid-State Rechargeable Lithium Batteries. *Nano Energy* **2017**, *33*, 363−386.
(7) Meyer, W. H. Polymer Electrolytes for Lithium-Ion Batteries. *Adv. Mater.* **1998**, *10*, 439−448.
(8) Zhang, H.; Li, C.; Piszcz, M.; Coya, E.; Rojo, T.; Rodriguez-Martinez, L. M.; Armand, M.; Zhou, Z. Single Lithium-Ion Conducting Solid Polymer Electrolytes: Advances and Perspectives. *Chem. Soc. Rev.* **2017**, *46*, 797−815.
(9) Lin, K.-J.; Li, K.; Maranas, J. K. Differences between Polymer/Salt and Single Ion Conductor Solid Polymer Electrolytes. *RSC Adv.* **2013**, *3*, 1564−1571.
(10) Sinha, K.; Maranas, J. K. Segmental Dynamics and Ion Association in PEO-Based Single Ion Conductors. *Macromolecules* **2011**, *44*, 5381−5391.
(11) Sinha, K.; Wang, W. Q.; Winey, K. I.; Maranas, J. K. Dynamic Patterning in PEO-Based Single Ion Conductors for Li Ion Batteries. *Macromolecules* **2012**, *45*, 4354−4362.
(12) O'Reilly, M. V.; Masser, H.; King, D. R.; Painter, P. C.; Colby, R. H.; Winey, K. I.; Runt, J. Ionic Aggregate Dissolution and Conduction in a Plasticized Single-Ion Polymer Conductor. *Polymer* **2015**, *59*, 133−143.
(13) Eisenberg, A.; Kim, J.-S. *Introduction to Ionomers*; Wiley Interscience: New York, 1998.
(14) Zhang, L.; Brostowitz, N. R.; Cavicchi, K. A.; Weiss, R. A. Perspective: Ionomer Research and Applications. *Macromol. React. Eng.* **2014**, *8*, 81−99.
(15) Middleton, L. R.; Winey, K. I. Nanoscale Aggregation in Acid- and Ion-Containing Polymers. *Annu. Rev. Chem. Biomol. Eng.* **2017**, *8*, 499−523.
(16) Deschanel, S.; Greviskes, B. P.; Bertoldi, K.; Sarva, S. S.; Chen, W.; Samuels, S. L.; Cohen, R. E.; Boyce, M. C. Rate Dependent Finite Deformation Stress-Strain Behavior of an Ethylene Methacrylic Acid Copolymer and an Ethylene Methacrylic Acid Butyl Acrylate Copolymer. *Polymer* **2009**, *50*, 227−235.
(17) Zhou, N. C.; Chan, C. D.; Winey, K. I. Reconciling STEM and X-Ray Scattering Data to Determine the Nanoscale Ionic Aggregate Morphology in Sulfonated Polystyrene Ionomers. *Macromolecules* **2008**, *41*, 6134−6140.
(18) Choi, U. H.; Liang, S.; Chen, Q.; Runt, J.; Colby, R. H. Segmental Dynamics and Dielectric Constant of Polysiloxane Polar Copolymers as Plasticizers for Polymer Electrolytes. *ACS Appl. Mater. Interfaces* **2016**, *8*, 3215−3225.
(19) Jin, X.; Zhang, S.; Runt, J. Broadband Dielectric Investigation of Amorphous Poly(Methyl Methacrylate)/Poly(Ethylene Oxide) Blends. *Macromolecules* **2004**, *37*, 8110−8115.
(20) Tudryn, G. J.; O'Reilly, M. V.; Dou, S.; King, D. R.; Winey, K. I.; Runt, J.; Colby, R. H. Molecular Mobility and Cation Conduction in Polyether-Ester-Sulfonate Copolymer Ionomers. *Macromolecules* **2012**, *45*, 3962−3973.
(21) Dou, S.; Zhang, S.; Klein, R. J.; Runt, J.; Colby, R. H. Synthesis and Characterization of Poly(Ethylene Glycol)-Based Single-Ion Conductors. *Chem. Mater.* **2006**, *18*, 4288−4295.
(22) Lu, M.; Runt, J.; Painter, P. An Infrared Spectrocopic Study of a Polyester Copolymer Ionomer Based on Poly(Ethylene Oxide). *Macromolecules* **2009**, *42*, 6581−6587.
(23) Wang, J.-H. H.; Yang, C. H.-C.; Masser, H.; Shiau, H.-S.; O'Reilly, M. V.; Winey, K. I.; Runt, J.; Painter, P. C.; Colby, R. H. Ion States and Transport in Styrenesulfonate Methacrylic PEO 9 Random Copolymer Ionomers. *Macromolecules* **2015**, *48*, 7273−7285.
(24) Fragiadakis, D.; Dou, S.; Colby, R. H.; Runt, J. Molecular Mobility and Li(+) Conduction in Polyester Copolymer Ionomers Based on Poly(Ethylene Oxide). *J. Chem. Phys.* **2009**, *130*, No. 064907.
(25) Fragiadakis, D.; Dou, S.; Colby, R. H.; Runt, J. Molecular Mobility, Ion Mobility, and Mobile Ion Concentration in Poly-(Ethylene Oxide)-Based Polyurethane Ionomers. *Macromolecules* **2008**, *41*, 5723−5728.
(26) He, R.; Kyu, T. Effect of Plasticization on Ionic Conductivity Enhancement in Relation to Glass Transition Temperature of Crosslinked Polymer Electrolyte Membranes. *Macromolecules* **2016**, *49*, 5637−5648.
(27) Bamford, D.; Reiche, A.; Dlubek, G.; Alloin, F.; Sanchez, J. Y.; Alam, M. A. Ionic Conductivity, Glass Transition, and Local Free Volume in Poly(Ethylene Oxide) Electrolytes: Single and Mixed Ion Conductors. *J. Chem. Phys.* **2003**, *118*, 9420−9432.
(28) Webb, M. A.; Jung, Y.; Pesko, D. M.; Savoie, B. M.; Yamamoto, U.; Coates, G. W.; Balsara, N. P.; Wang, Z.-G.; Miller, T. F. Systematic Computational and Experimental Investigation of Lithium-Ion Transport Mechanisms in Polyester-Based Polymer Electrolytes. *ACS Cent. Sci.* **2015**, *1*, 198−205.
(29) Schauser, N. S.; Sanoja, G. E.; Bartels, J. M.; Jain, S. K.; Hu, J. G.; Han, S.; Walker, L. M.; Helgeson, M. E.; Seshadri, R.; Segalman, R. A. Decoupling Bulk Mechanics and Mono- and Multivalent Ion Transport in Polymers Based on Metal-Ligand Coordination. *Chem. Mater.* **2018**, *30*, 5759−5769.
(30) Morris, M. A.; An, H.; Lutkenhaus, J. L.; Epps, T. H. Harnessing the Power of Plastics: Nanostructured Polymer Systems in Lithium-Ion Batteries. *ACS Energy Lett.* **2017**, *2*, 1919−1936.
(31) Park, M. J. Confinement-Entitled Morphology and Ion Transport in Ion-Containing Polymers. *Mol. Syst. Des. Eng.* **2019**, *4*, 239−251.
(32) Baughman, T. W.; Chan, C. D.; Winey, K. I.; Wagener, K. B. Synthesis and Morphology of Well-Defined Poly (Ethylene-Co-Acrylic Acid) Copolymers. *Macromolecules* **2007**, *40*, 6564−6571.
(33) Choi, U.; Robert Middleton, L.; Soccio, M.; Francisco Buitrago, C.; Aitken, B. S.; Masser, H.; Wagener, K. B.; Winey, K. I.; Runt, J. Dynamics of Precise Ethylene Ionomers Containing Ionic Liquid Functionality. *Macromolecules* **2015**, *48*, 410−420.
(34) Seitz, M. E.; Chan, C. D.; Opper, K. L.; Baughman, T. W.; Wagener, K. B.; Winey, K. I. Nanoscale Morphology in Precisely Sequenced Poly(Ethylene-Co-Acrylic Acid) Zinc Ionomers. *J. Am. Chem. Soc.* **2010**, *132*, 8165−8174.
(35) Buitrago, C. F.; Jenkins, J. E.; Opper, K. L.; Aitken, B. S.; Wagener, K. B.; Alam, T. M.; Winey, K. I. Room Temperature Morphologies of Precise Acid- and Ion-Containing Polyethylenes. *Macromolecules* **2013**, *46*, 9003−9012.

(36) Buitrago, C. F.; Bolintineanu, D. S.; Seitz, M. E.; Opper, K. L.; Wagener, K. B.; Stevens, M. J.; Frischknecht, A. L.; Winey, K. I. Direct Comparisons of X-Ray Scattering and Atomistic Molecular Dynamics Simulations for Precise Acid Copolymers and Ionomers. *Macromolecules* **2015**, *48*, 1210−1220.
(37) Li, H.; Caire da Silva, L.; Schulz, M. D.; Rojas, G.; Wagener, K. B. A. Review of How to Do an Acyclic Diene Metathesis Reaction. *Polym. Int.* **2017**, *66*, 7−12.
(38) Wagener, K. B.; Boncella, J. M.; Nel, J. G. Acyclic Diene Metathesis (ADMET) Polymerization. *Macromolecules* **1991**, *24*, 2649−2657.
(39) Schulz, M. D.; Wagener, K. B. Precision Polymers through ADMET Polymerization. *Macromol. Chem. Phys.* **2014**, *215*, 1936−1945.
(40) Hopkins, T. E.; Wagener, K. B. Bio-Olefins via Condensation Metathesis Chemistry. *J. Mol. Catal. A: Chem.* **2004**, *213*, 93−99.
(41) da Silva, L. C.; Rojas, G.; Schulz, M. D.; Wagener, K. B. Acyclic Diene Metathesis Polymerization: History, Methods and Applications. *Prog. Polym. Sci.* **2017**, *69*, 79−107.
(42) Hall, L. M.; Seitz, M. E.; Winey, K. I.; Opper, K. L.; Wagener, K. B.; Stevens, M. J.; Frischknecht, A. L. Ionic Aggregate Structure in Ionomer Melts: Effect of Molecular Architecture on Aggregates and the Ionomer Peak. *J. Am. Chem. Soc.* **2012**, *134*, 574−587.
(43) Hall, L. M.; Stevens, M. J.; Frischknecht, A. L. Effect of Polymer Architecture and Ionic Aggregation on the Scattering Peak in Model Ionomers. *Phys. Rev. Lett.* **2011**, *106*, 1−4.
(44) Middleton, L. R.; Trigg, E. B.; Schwartz, E.; Opper, K. L.; Baughman, T. W.; Wagener, K. B.; Winey, K. I. Role of Periodicity and Acid Chemistry on the Morphological Evolution and Strength in Precise Polyethylenes. *Macromolecules* **2016**, *49*, 8209−8218.
(45) Middleton, L. R.; Trigg, E. B.; Yan, L.; Winey, K. I. Deformation-Induced Morphology Evolution of Precise Polyethylene Ionomers. *Polymer* **2018**, *144*, 184−191.
(46) Yan, L.; Bustillo, K. C.; Panova, O.; Minor, A. M.; Winey, K. I. Solution-Grown Crystals of Precise Acid- and Ion-Containing Polyethylenes. *Polymer* **2018**, *135*, 111−119.
(47) Trigg, E. B.; Gaines, T. W.; Maréchal, M.; Moed, D. E.; Rannou, P.; Wagener, K. B.; Stevens, M. J.; Winey, K. I. Self-Assembled Highly Ordered Acid Layers in Precisely Sulfonated Polyethylene Produce Efficient Proton Transport. *Nat. Mater.* **2018**, *17*, 725−731.
(48) Trigg, E. B.; Stevens, M. J.; Winey, K. I. Chain Folding Produces a Multilayered Morphology in a Precise Polymer: Simulations and Experiments. *J. Am. Chem. Soc.* **2017**, *139*, 3747−3755.
(49) Cui, K.; Ma, Z.; Tian, N.; Su, F.; Liu, D.; Li, L. Multiscale and Multistep Ordering of Flow-Induced Nucleation of Polymers. *Chem. Rev.* **2018**, *118*, 1840−1886.
(50) Bolintineanu, D. S.; Stevens, M. J.; Frischknecht, A. L. Atomistic Simulations Predict a Surprising Variety of Morphologies in Precise Ionomers. *ACS Macro Lett.* **2013**, *2*, 206−210.
(51) Frischknecht, A. L.; Winey, K. I. The Evolution of Acidic and Ionic Aggregates in Ionomers during Microsecond Simulations. *J. Chem. Phys.* **2019**, *150*, No. 064901.
(52) Hall, L. M.; Stevens, M. J.; Frischknecht, A. L. Dynamics of Model Ionomer Melts of Various Architectures. *Macromolecules* **2012**, *45*, 8097−8108.
(53) Ting, C. L.; Stevens, M. J.; Frischknecht, A. L. Structure and Dynamics of Coarse-Grained Ionomer Melts in an External Electric Field. *Macromolecules* **2015**, *48*, 809−818.
(54) Ting, C. L.; Sorensen-Unruh, K. E.; Stevens, M. J.; Frischknecht, A. L. Nonequilibrium Simulations of Model Ionomers in an Oscillating Electric Field. *J. Chem. Phys.* **2016**, *145*, No. 044902.
(55) Lin, K.-J.; Maranas, J. K. Superionic Behavior in Polyethylene-Oxide-Based Single-Ion Conductors. *Phys. Rev. E* **2013**, *88*, No. 052602.
(56) Sampath, J.; Hall, L. M. Impact of Ionic Aggregate Structure on Ionomer Mechanical Properties from Coarse-Grained Molecular Dynamics Simulations. *J. Chem. Phys.* **2017**, *147*, No. 134901.
(57) Trigg, E. B.; Tiegs, B. J.; Coates, G. W.; Winey, K. I. High Morphological Order in a Nearly Precise Acid-Containing Polymer and Ionomer. *ACS Macro Lett.* **2017**, *6*, 947−951.
(58) Tiegs, B. J. *Succinic Anhydride-Alcohols: A New Class of Autocatalytic Self-Polymerizable Monomers via Carbonylation of Epoxy-Alcohols*; Cornell University: Ithaca, New York, 2016.
(59) Painter, P. C.; Brozoski, B. A.; Coleman, M. M. FTIR Studies of Calcium and Sodium Ionomers Derived from an Ethylene−Methacrylic Acid Copolymer. *J. Polym. Sci. Polym. Phys. Ed.* **1982**, *20*, 1069−1080.
(60) Bolintineanu, D. S.; Stevens, M. J.; Frischknecht, A. L. Influence of Cation Type on Ionic Aggregates in Precise Ionomers. *Macromolecules* **2013**, *46*, 5381−5392.
(61) Lueth, C. A.; Bolintineanu, D. S.; Stevens, M. J.; Frischknecht, A. L. Hydrogen-Bonded Aggregates in Precise Acid Copolymers. *J. Chem. Phys.* **2014**, *140*, No. 054902.
(62) Yan, L.; Rank, C.; Mecking, S.; Winey, K. I. Gyroid and Other Ordered Morphologies in Single-Ion Conducting Polymers and Their Impact on Ionic Conductivity. *J. Am. Chem. Soc.* **2020**, *142*, 857−866.
(63) Rank, C.; Yan, L.; Mecking, S.; Winey, K. I. Periodic Polyethylene Sulfonates from Polyesterification: Bulk and Nanoparticles Morphologies and Ionic Conductivities. *Macromolecues* **2019**, *52*, 8466−8475.

https://dx.doi.org/10.1021/acs.macromol.9b02220
Macromolecules 2020, 53, 1777−1784